PHILOSOPHICAL TRANSACTIONS A

royalsocietypublishing.org/journal/rsta

Research

Cite this article: McCormack FS, Stål T, Shao N, MacKie E, Fabela Hinojosa A, Lösing M, Roberts J, Ehrenfeucht S, Dow C. 2026 Synthetic bed topographies for Antarctica and their utility in ice sheet modelling. *Phil. Trans. R. Soc. A* **384**: 20240537.
https://doi.org/10.1098/rsta.2024.0537

Received: 7 July 2025
Accepted: 22 September 2025

One contribution of 16 to a Theo Murphy meeting issue 'Next generation ice-sheet bed measurements'.

Subject Areas:
glaciology

Keywords:
Antarctica, bed topography, ice sheet modelling

Author for correspondence:
Felicity S. McCormack
e-mail: felicity.mccormack@monash.edu

Electronic supplementary material is available online at https://doi.org/10.6084/m9.figshare.c.8426934.

THE ROYAL SOCIETY PUBLISHING

Synthetic bed topographies for Antarctica and their utility in ice sheet modelling

Felicity S. McCormack[1], Tobias Stål[2,4], Niya Shao[5], Emma MacKie[6], Ana Fabela Hinojosa[1], Mareen Lösing[4,7], Jason Roberts[8,3], Shivani Ehrenfeucht[9] and Christine Dow[10]

[1]Securing Antarctica's Environmental Future, School of Earth, Atmosphere & Environment, Monash University, Clayton, Kulin Nations, Victoria, Australia
[2]School of Natural Sciences, and [3]Australian Antarctic Program Partnership, Institute for Marine and Antarctic Studies, University of Tasmania, Hobart, Tasmania, Australia
[4]The Australian Centre for Excellence in Antarctic Science (ACEAS), Hobart, Australia
[5]Department of Geological Sciences, University of Florida, Gainesville, FL, USA
[6]University of Florida, Gainesville, FL, USA
[7]School of Earth and Oceans, University of Western Australia, Perth, Western Australia, Australia
[8]Australian Antarctic Division, Kingston, Tasmania, Australia
[9]Potsdam Institute for Climate Impact Research, Potsdam, Brandenburg, Germany
[10]Geography and Environmental Management, University of Waterloo, Waterloo, Ontario, Canada

FSM, 0000-0002-2324-2120; NS, 0009-0003-3298-7719

Bed topography is a key control on the evolution of the Antarctic Ice Sheet, influencing ice flow, grounding line retreat and the rate and timing of ice mass loss. To assess the sensitivity of ice sheet evolution to bed variability in ice sheet models, synthetic gridded bed topography datasets are often used. Here, we review methods commonly used to generate synthetic beds, their associated uncertainties and the influence of the approach on the characteristics of the resulting bed. Using the Aurora Subglacial Basin in East Antarctica as a case study, we evaluate the impact of five synthetic bed generation methods on projected ice mass loss under a high emission scenario. Sea-level rise estimates vary by up to 11% (SSP5-8.5 forcing scenario) and 32% (RCP2.6) at 2300 CE when basal friction coefficients from the friction law are optimized for each bed, and by up to 23% (SSP5-8.5) and

51% (RCP2.6) at 2300 CE when using non-optimized coefficients. Our results highlight the importance of relatively small bed variations on the timing and extent of grounding line retreat and the need for process-informed representation of the basal friction in decadal- to centennial-scale sea-level projections.

This article is part of the Theo Murphy meeting issue 'Next generation ice-sheet bed measurements'.

1. Introduction

Bed topography is one of the most critical variables for controlling the evolution of the Antarctic Ice Sheet. At a regional to sector scale, bed topography controls the magnitude and timing of ice volume changes by influencing the ice velocity and rate of grounding line retreat. This influence can be due to the role of pinning points [1–5], or via the bed slope or curvature that influences glacier susceptibility to instabilities [6–9]. Ice–bed interactions provide resistance to flow [10], including through pinning points [11], influencing buttressing [12,13] and determining the relative contributions of deformation and sliding to the overall column-averaged speed [14–16]. Frictional heating at the base of the ice sheet regulates the basal thermal regime [17,18] and production of liquid meltwater, which feeds the subglacial hydrological system [19–23]. Sub-ice shelf bathymetry influences the supply of ocean water masses to the ice shelf cavity [24], and ice shelf and grounding line ocean-driven melt rates [25,26]. Bed features influence the direction and magnitude (i.e. by modifying the total bed surface area) of heat transfer from the solid Earth to the ice sheet [27,28]. Bed topography is hence a critically important boundary condition for ice sheet dynamics, and by extension, numerical ice sheet modelling.

The primary method of measuring bed topography is via airborne radar surveys, which have provided over 82 million data points across Antarctica since the 1950s [29]. Ground-based radar and seismic surveys can also provide detailed bed measurements (e.g. [30,31]), but are highly localized and not as widely available as airborne radar. Hence, despite its importance, bed topography remains sparsely sampled across Antarctica, and particularly in critical regions: close to the present-day grounding line, and within upstream regions into which the grounding line may retreat in the coming decades to centuries. For example, approximately 10% of the present-day grounding line has a data point within 1 km, and 59% of the grounding line has a data point within 5 km [32]. Compounding issues of insufficient survey coverage and radar reflections from off-target features in regions of steep topography—characteristic of deepened troughs in coastal zones—may lead to clutter, mask the ability to determine where the ice–bed interface is, and introduce uncertainties. Errors in the bed consequently propagate in ice sheet modelling simulations [33–35]. Bathymetry within ice shelf cavities is also particularly poorly known. These regions are inaccessible to most ship-borne platforms [36], and high-fidelity sub-ice shelf submersible surveys are limited to small regions. While inversion of gravity data collected from airborne surveys provides some constraints on cavity bathymetry [37–40], large uncertainties in the density of the geological substrate may result in limited accuracy for the inferred cavity geometry. In addition, the limited achievable horizontal and vertical resolution of the gravity inversion impacts confidence in these estimates at the scales required for ocean modelling over broad regions (e.g. [37]).

Ice sheet modelling typically relies on gridded bed topography datasets that use some method of interpolation to gap-fill sparsely sampled radar-derived bed topography. However, the approach used to generate the bed topography influences how realistically features are captured in the resulting dataset. Some methods, such as Kriging, result in overly smooth beds, producing unrealistic estimates of topographic roughness [41,42], and can lead to large simulated mass flux

divergence due to inconsistencies between model fields [35]. Alternative approaches to interpolating gridded bed topographies have been proposed to circumvent these issues. These encompass mass conservation, geostatistical simulation and geophysical approaches (i.e. gravity inversion in ice shelf cavities), or approaches that combine multiple methods or datasets, including machine learning. The resulting gridded bed topography datasets are 'synthetic' in that they rely on different approaches to gap-fill or interpolate measured bed data.

The aim of this study is to examine the utility of synthetic bed topographies in ice sheet modelling applications. We define utility as allowing us to either accurately characterize ice sheet properties or dynamics (e.g. for studies that produce sea-level rise projections) or to provide new insights into ice sheet processes that may be poorly understood. We first describe the objectives that guide the generation of synthetic bed topographies, reviewing the approaches used and how they assess uncertainty. Focusing on the Aurora Subglacial Basin, East Antarctica, we present an ice sheet modelling case study evaluating the sensitivity of projected sea-level contributions to bed topographies generated using different approaches. We finish by discussing where such ensembles may be useful in constraining key unknowns in ice sheet modelling.

2. Methods to generate synthetic bed topographies

Synthetic topographies are typically generated to meet one of two primary objectives (figure 1): (i) to preserve elevation accuracy, ensuring the bed matches observed values where available and interpolates appropriately elsewhere, and (ii) to preserve statistical texture, such as covariance structure, so that roughness characteristics are spatially consistent. While these goals are not necessarily mutually exclusive (the true bed being an example that is both elevation- and texture-preserving), most methods prioritize one objective over the other to varying degrees. The utility of a given synthetic bed is influenced by its design objective, which, in turn, influences the types of ice sheet modelling questions it is most suited to be used for.

Below, we review common approaches for generating synthetic bed topographies, their placement along the elevation–texture spectrum and the associated methods for estimating uncertainty.

(a) Traditional interpolation methods

(i) Mathematical approaches

Among the most straightforward approaches to generating synthetic bed topographies using non-geostatistical interpolation methods are mathematical functions used to gap-fill unsampled locations using nearby bed observations—i.e. generating elevation-preserving bed topographies. Interpolation methods include linear, inverse-distance weighted, spline, bilinear/bicubic and nearest neighbour interpolation. No spatial model is assumed in these approaches, such that proximity to observations is the primary determinant of the resultant bed. Bed topography datasets generated using these approaches include: Bedmap1 [43], which uses an inverse-cubed weighted algorithm and Bedmap2 [44] and Bedmap3 [29,45], which use the Topo-to-raster method (formerly TopoGrid) from ANUDEM [46] implemented in ArcGIS. Topo-to-raster uses thin plate splines to produce a smooth surface through the use of iterative finite difference interpolation. Uncertainty in the interpolated topography in Bedmap3, which comprises 93% of the grounded ice, is calculated heuristically as a function of the distance to the closest topography measurement. This heuristic relationship between uncertainty and distance is derived from the difference between the new observations added in Bedmap3 and the interpolated topography in Bedmap2.

Many traditional approaches generate only a single bed realization, where specific parameter choices can strongly influence the resulting topography. In such cases, uncertainties are typically addressed in an ad hoc or heuristic manner. To overcome these limitations, ensemble-based methods have been proposed that allow for more robust assessment and propagation of uncertainty.

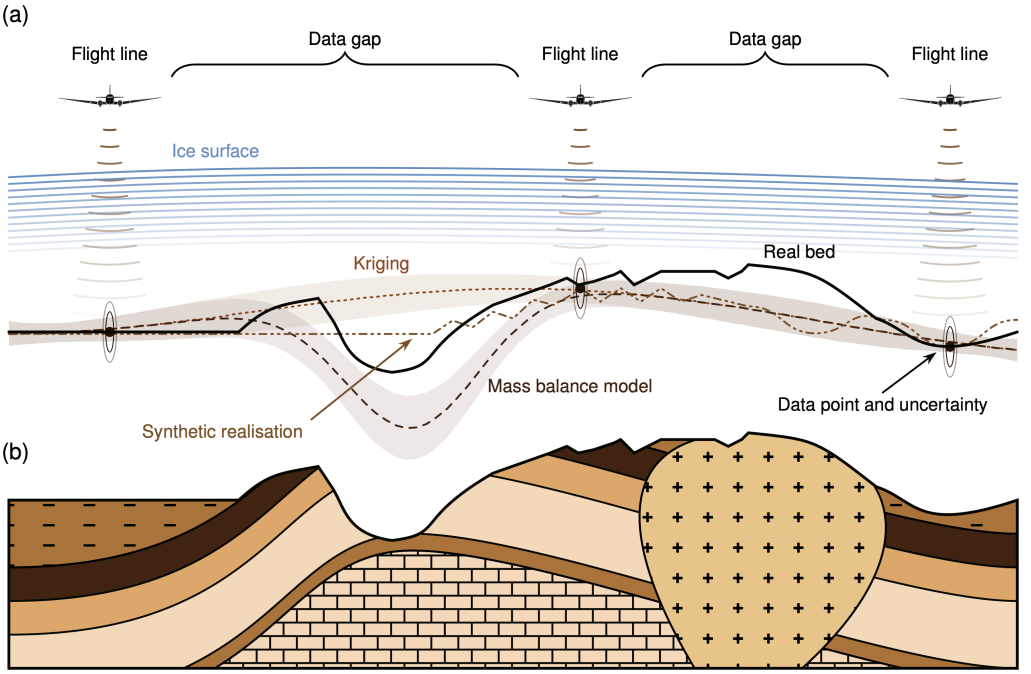

Figure 1. Schematic representing the information that is used to generate bed topographies. (a) Realizations of synthetic bed topographies in regions of data gaps between flight lines, highlighting differences between beds generated to preserve elevation (e.g. Bedmap3, SMUG), for example using methods of Kriging or mass conservation, which may incorporate satellite observations of surface velocity; and beds generated to preserve texture (e.g. MCMC), for example using geostatistical methods, which consider the shape of the bed at the flight lines. (b) Other information at the bed, including the bed type (e.g. hard or soft geological substrates) and the landforms formed by past subglacial and periglacial processes, which can influence both the generation of a synthetic bed topography, depending on the method used, and the evolution of the ice sheet dynamics simulated in a model, as a function of the representation of different processes and parameter values.

One such example is the stochastic meshless uncertainty gridding (SMUG, [47]) algorithm. SMUG is a point-wise interpolation scheme based on a local Taylor series, which produces a robust estimate of both the field being interpolated (here bed topography) and the associated uncertainty. Spatial derivatives required by the Taylor series are calculated via a high-precision meshless algorithm [48], using a pool of suitable nearby neighbouring observations for both the Taylor series origin and the calculation of the derivatives. An ensemble approach is used to estimate the interpolated value and the uncertainty, with points being drawn randomly from the neighbour pool for both the Taylor series origin and derivative calculation, and robust statistical methods are used to calculate the ensemble central tendency and spread. The method can be applied to both bed topography and texture (i.e. the characteristics of the bed roughness and variability across spatial scales) fields independently.

The above approaches are commonly used in generating bed topographies, including in non-glaciated environments. A key limitation is the neglect of accounting for spatial autocorrelation, which can lead to overly smoothed or unrealistic bed topographies, particularly in sparsely sampled regions [41,42]. Furthermore, common interpolation methods are typically used to map gridded bed products onto ice sheet model meshes. Although these interpolation distances are typically much smaller, with correspondingly smaller additional errors and uncertainties than in the generation of the original bed topography, this can introduce a second layer of uncertainties in the meshed bed topographies that can propagate in ice sheet modelling (e.g. see discussion in [2]).

(ii) Linear perturbation theory

Linear perturbation theory has been used to generate bed topographies by deriving transfer functions in Fourier space that link ice surface velocity and elevation to basal properties. For example, building on [49,50], recent studies [51,52] applied steady-state linear perturbation theory and the shallow ice approximation to the full-Stokes equations to generate bed topography datasets for Thwaites and Pine Island Glaciers, West Antarctica. This approach assumes that ice is a linear viscous fluid (i.e. a Newtonian fluid), flowing at a constant speed, and solves the resulting overdetermined system via weighted least squares. The resulting beds realistically capture medium-wavelength features beneath fast-flowing ice but are associated with higher uncertainty in areas where the shelfy-stream approximation (SSA) to the full-Stokes equations does not hold, such as areas with steep topography. Hence, this method generates bed topographies that aim to realistically capture landforms and is therefore between the end members (i.e. elevation-preserving or texture-preserving) on the methodological spectrum.

The topography produced by linear perturbation is subject to several uncertainties, including parameters used in the inversion (e.g. mean ice thickness and mean basal slipperiness), limitations in capturing short-wavelength bed features that do not propagate to the surface and the linearization approximation (ice is a non-Newtonian fluid). The method divides the domain into discrete regions, solving for topography in each region independently. To estimate uncertainty, the standard deviation of topography in overlapping regions is computed; uncertainties related to the linearization approximation, and to some extent, the inversion parameters, are also quantified.

(iii) Mass conservation

The mass conservation method uses the governing equation for the conservation of mass to reconstruct bed topography in regions of sparse bed measurements [53,54]. Using observed estimates of ice surface velocity and surface mass balance inputs, the mass conservation method solves for ice thickness via the ice flux divergence term ($\nabla \cdot H\bar{\mathbf{v}}$) and ice surface elevation. The method is most suitable in regions of relatively fast flow (i.e. where the ice surface velocity is greater than or equal to 50 m yr^{-1}) and where there is a constant ratio of surface to column-averaged velocities (i.e. where SSA applies). Outside these regions, uncertainties in the mass flux term become large, and the method is less reliable.

Mass conservation has been used to generate bed topographies for both the Antarctic and Greenland Ice Sheets. The BedMachine Antarctic and Greenland datasets [53–55] are among the most widely used topographies in ice sheet modelling applications (e.g. in the Ice Sheet Model Intercomparison Project for CMIP6; [56–60]). To generate these datasets, the mass conservation method was improved to assimilate radar-derived ice thickness estimates [61], such that the resulting bed topographies are close to elevation-preserving.

The uncertainties in BedMachine Antarctica v. 3 [54,62] are estimated using a combination of approaches. In fast-flowing regions, uncertainties are estimated by solving a linearized mass conservation equation propagated both downstream and upstream of radar flight lines, taking into account uncertainties in surface velocity and surface mass balance observational estimates. In slow-moving regions, uncertainties are heuristic, with errors assumed to grow linearly as a function of the distance from the nearest measurement, and capped at 1000 m.

An alternative mass conservation approach is TELVIS (thickness estimation by a Lagrangian validated interpolation scheme; [63]). TELVIS is a streamline-based mass conservation method that uses ice surface slope and accumulation to infer ice thickness under local mass balance assumptions. This method interpolates along surface streamlines between observations, resulting in low variability along streamlines, but (locally) high variability across flow. To address this issue, Gaussian smoothing is applied to the interpolated topography, such that bed measurements are not necessarily honoured. This method has been used to generate bed topographies in the Aurora Subglacial Basin, East Antarctica. Uncertainties are estimated at each observational point using the TELVIS algorithm in separate computations. That is, for each point, all observational

data within a 5 km radius—including the point itself—are excluded from the calculation, and the uncertainty is computed as the difference between the TELVIS-predicted ice thickness estimate and the observed value at that point.

(b) Geostatistical methods

Geostatistics comprises stochastic and spatial statistics-based methods to generate bed topography datasets and associated uncertainties that are consistent with observed data and known characteristics of the bed, including its texture, roughness or correlation structure [64]. Geostatistical approaches can be categorized into deterministic estimation-based methods (e.g. Kriging), simulation-based methods (e.g. sequential Gaussian simulation (SGS), multiple-point direct sampling, Markov chain Monte Carlo (MCMC)) or hybrid/advanced methods (e.g. geostatistical inversion and combined geostatistical/machine learning approaches).

(i) Kriging

The Kriging family of methods (ordinary, universal, simple, indicator, co-, regression or Bayesian Kriging) are forms of Gaussian process regression that use spatial covariance information to generate bed estimates at unsampled locations (i.e. Kriging is an elevation-preserving method). Ordinary, universal and regression Kriging incorporate trends or regression models to integrate the non-stationarity of the data. The objective of Kriging is to optimize local accuracy and interpolate values in such a way that the estimation variance is minimized [65]. An advantage of Kriging is that it produces an estimation variance at each interpolated grid cell, providing a robust uncertainty estimate. Furthermore, although Kriging is mathematically elegant, it can generate 'bulls-eye' patterning, whereby systematic, spurious sinks or conical features are introduced into the bed topography. Kriging, by definition, also averages radar bed measurements to perform interpolations, which causes smoothing. As such, Kriging does not reproduce the spatial covariance of observations.

(ii) Geostatistical simulation

While Kriging prioritizes interpolation accuracy at the cost of realistic spatial characteristics, geostatistical simulation is designed to reproduce the spatial structure observed in the data [66]. This approach involves generating multiple realizations of bed topography that are conditioned to available measurements and exhibit realistic roughness [64]—i.e. texture-preserving. The resulting ensemble of realizations provides a quantitative measure of uncertainty and enables the propagation of bed uncertainty into downstream models. Geostatistical simulation methods typically fall into two main categories: (i) SGS, and (ii) multiple-point statistics (MPS). SGS is the stochastic counterpart to Kriging and is built on the same system of equations. In theory, the mean and variance of an SGS ensemble approximate the Kriging estimate and variance. SGS approaches can account for spatial trends, anisotropy and even heterogeneous roughness in bed topography [42]. MPS methods, by contrast, are non-parametric and rely on representative training images to model complex spatial patterns [67]. In the context of subglacial topography, MPS uses densely surveyed bed regions and seafloor bathymetry as training data to fill in data gaps [41,68,69]. While MPS excels at simulating complex geological textures, its effectiveness depends critically on the availability, quality and appropriateness of training images.

(iii) Geostatistical inversion

The advantages of geostatistical simulation and geophysical inversion (e.g. gravity inversion for bathymetry) can be combined through geostatistical inversion [70–73]. Typically, this involves some sort of MCMC approach where geostatistical realizations are iteratively perturbed until

forward-modelled synthetic data match the measurements. This framework is advantageous because it allows for the sampling of the parameter space and does not require the inverse problem to be solved directly, making it well suited for non-unique, nonlinear inverse problems. This approach has recently been used to generate bed topography ensembles that are both texture-preserving and consistent with observed fields (i.e. ice surface velocity, elevation and surface mass balance; [74]). The ensemble of topographies generated with MCMC can be considered as a set of samples from the posterior distribution defined based on the physical constraints. This approach captures the uncertainties associated with different solutions to the same governing equation, such as mass conservation. The ensemble approach enables uncertainties in bed topography to be systematically propagated in ice sheet model simulations.

(c) Machine learning methods

Machine learning, including physics-informed and data-driven approaches, has more recently been used to generate bed topography datasets. As with the approaches outlined above, machine learning models can leverage a range of input data, including ice surface velocity and elevation (and trends), radar observations and surface mass balance, to estimate the underlying bed elevation.

Various machine learning models have been applied to generating bed topography datasets [75–78]. Algorithms, such as gradient-boosted decision trees (e.g. XGBoost; [77]), can handle structured data, identifying spatial relationships between features at the surface and the ice–bed interface (i.e. similar to linear perturbation theory). Deep learning models, particularly convolutional neural networks, are designed to identify spatial hierarchies in gridded datasets and hence resolve features across spatial scales. More recently, machine learning approaches that combine multiple input datasets, including radar-derived bed elevation measurements, as well as surface datasets (velocity, elevation), are being developed. One such approach—DeepBedMap—adapts the enhanced super-resolution generative adversarial network algorithm to generate a very high-resolution (250 m) bed elevation model [76]. In addition to the higher resolution than many classically interpolated products, an advantage of this approach is in producing bed roughness at a fine scale that aligns more closely with the expected texture of the bed elevation measurements. Building on its application to internal ice layers and to better handle sparse and irregularly sampled data, the graph neural network approach has also been utilized for Antarctic bed elevation applications [79]. The advantage of this approach is its ability to learn from patterns within a neighbourhood of points, with good skill in representing patterns in the bed elevation. Across these studies, training labels are typically gridded radar-derived bed elevations or pre-trained on the external ArcticDEM to infer Antarctic bed. Reported validation strategies range from standard train/test splits to spatial cross-validations and product benchmarking. Full methodological specifics are detailed in the original articles.

Although not yet applied in glaciology, other fields such as groundwater hydrology have demonstrated that integrating geostatistical techniques (e.g. universal Kriging), structured data processing and deep learning can improve the realism of machine learning datasets [80] by enforcing physically consistent relationships between inputs and predictions. However, the focus on preserving large-scale elevation structure could also lead to small-scale structures being overly smoothed, highlighting a potential trade-off between physical consistency and high-frequency detail, particularly in sparsely sampled regions.

Uncertainties in bed topographies derived from machine learning models arise from multiple factors, including unevenness in training data coverage (e.g. radar line density), input feature selection and assumptions in the model architecture. Quantifying these uncertainties is critical, yet often remains ad hoc. Evaluation metrics like the root mean square error provide a global error estimate but cannot adequately quantify spatially variable uncertainty. Ensemble modelling, cross-validation and uncertainty-aware architectures like Bayesian neural networks are increasingly used to estimate predictive uncertainty [81]; however, standardized approaches for quantifying

uncertainty remain limited. Moreover, neural networks often lack clearly defined optimization goals. In geostatistics, interpolation outcomes are typically explicit: optimizing local accuracy (i.e. elevation-preserving, as in Kriging) or spatial variability (i.e. texture-preserving, as in SGS). However, by contrast, neural networks often attempt to satisfy both objectives simultaneously, resulting in outputs that may be difficult to interpret.

(d) Joint inversions: disentangling bed topography and basal friction

In the preceding sections, we reviewed approaches to generating synthetic bed topographies through the assimilation of various data streams. The efficacy of some of the approaches outlined above is influenced by underlying assumptions about bed properties, including the basal friction coefficient field and the properties and processes that influence it. For example, methods that employ inversion typically assume a fixed spatial structure for the basal friction coefficient, which can lead to unresolved resistance at the bed being attributed to either friction or topography, without the capacity to distinguish between skin drag (frictional resistance) and form drag (arising from bed geometry). This is an issue that has been previously discussed in the literature [10], including in relation to locations where the bed topography is unresolved [82]. It can lead to significant errors in both bed topography and basal friction fields, especially in regions with sparse observations, complex basal processes or when other ice dynamics processes are poorly constrained [16,83].

An alternative approach is joint inversion (e.g. [84–89]), which simultaneously solves for both the bed topography and basal friction coefficient using surface observables (e.g. velocity and elevation), allowing for a more continuously discretized partitioning between processes that influence basal drag. Such an approach also reduces the risk of compensating errors, including where friction and bed elevation adjust in offsetting ways to fit surface constraints. One approach to joint inversion is via ensemble-based Bayesian frameworks (e.g. [84]), which allow quantification of uncertainties and correlations between the inverted fields, helping to identify regions where drag attribution is ambiguous or poorly constrained. Another approach is via snapshot (i.e. one point in time) or time-dependent data assimilation. The latter shows considerable advantage in taking into account the transient nature of both the fields that are being derived (e.g. transient effects on the friction coefficient) and the observables included in the assimilation (e.g. surface velocity and elevation). A more complete review of time-dependent data assimilation and the computational techniques used to perform it, such as automatic differentiation, is provided in [88].

As for all of the methodologies we have reviewed above that require treatment of the basal friction coefficient, joint inversion frameworks typically assume temporally static basal conditions. This limits their ability to represent transient processes in the basal friction field, such as evolving subglacial drainage, sediment transport or other changes associated with grounding line migration. Capturing such processes would require not only joint inversion but also time-dependent data assimilation (e.g. [88]) and more sophisticated treatment of subglacial processes (e.g. [90]). Nevertheless, joint inversion offers a promising pathway to more physically motivated representations of both bed topography and basal friction.

3. Ice sheet sensitivity to bed topography

Understanding the sensitivity of ice sheet evolution to bed topography has been a long-standing focus of ice sheet modelling studies. A common approach to assessing such sensitivity involves generating large ensembles of bed topography realizations, where variations in the bed are informed by uncertainty estimates (e.g. [1,91]) or by adding structured or random noise (e.g. [92,93]), and running prognostic ice sheet model simulations to evaluate differences in the ice sheet response to different bed topography realizations. Such ensemble-based approaches enable quantification of the influence of bed variations on key ice sheet variables. Ensemble approaches can

also be used to determine how well the bed must be constrained (i.e. to what level must uncertainty be reduced) to ensure that sea-level rise projections remain within a prescribed tolerance. This approach has been recently applied to the Thwaites Glacier catchment [1], where wavelet decomposition was used to construct an ensemble of bed realizations. The study found that to limit global sea-level rise uncertainty due to ice loss from the Thwaites catchment to ±2 cm would require constraining bed topography to within 8 m vertically and 2 km horizontally. Note, however, that this resolution requirement may vary for different Antarctic catchments.

An alternative approach to assessing ice sheet sensitivity to bed topography is via automatic differentiation [94,95], which quantifies the sensitivity of a model output to perturbations in a given independent input. This method characterizes spatial sensitivity and hence highlights where constraining estimates of an independent variable will be most valuable in constraining propagated uncertainties in the ice sheet evolution. For example, Utke *et al.* [94] showed that the ice volume above flotation in the Amundsen Sea Sector is largely insensitive to basal friction coefficient variations in the ice sheet interior, but highly sensitive within a few tens of kilometres upstream of the Pine Island and Thwaites Glacier grounding lines. Although automatic differentiation is gaining traction in glaciological applications, it has yet to be applied to assess sensitivities to bed topography.

Ensemble approaches and automatic differentiation provide complementary insights into ice sheet sensitivity. Ensemble approaches assess how uncertainties in bed topography of varying magnitudes and spatial structures influence ice sheet evolution. This is particularly useful for evaluating how errors in elevation or landform (i.e. elevation- versus texture-preserving bed topographies) might affect projections, and for determining the level of observational constraint required in different regions, as discussed above. By contrast, automatic differentiation identifies where the model is most sensitive to perturbations in the bed, independent of their actual magnitude or uncertainty. This makes it a powerful tool for locating regions where small errors—if present—could have relatively large effects on ice dynamics. The distinction between these two approaches is important when considering physical processes at the ice–bed interface. For example, a region with high form drag may show strong sensitivity to small-scale topographic undulations (e.g. pinning points), which a texture-preserving bed realization could better capture. Conversely, a region dominated by skin drag might exhibit lower sensitivity to topographic detail but higher sensitivity to friction-related processes. Ensemble methods can capture sensitivity resulting from both, but only automatic differentiation can precisely highlight the mesh pointwise impact of variations on the metric in question (e.g. flux over the grounding line). While our study is based on ensemble methods, future work would benefit from incorporating automatic differentiation to identify the regions and processes that could be targeted for improved realism of ice sheet model projections.

4. Assessing ice sheet sensitivity to bed variations: a case study of the Aurora Subglacial Basin

In this section, we assess the sensitivity of mass loss from the Aurora Subglacial Basin to bed topography using the ice-sheet and sea-level system model (ISSM; [96]). The Aurora Subglacial Basin is one of the most rapidly evolving catchments in East Antarctica [97,98], with ocean-driven ice shelf melt dominating its evolution [3,5,98]. Containing approximately 7 m of equivalent sea level, the Aurora Subglacial Basin has been the subject of several ICECAP (Investigating the Cryospheric Evolution of the Central Antarctic Plateau; [63]) surveys since 2008, resulting in approximately 9.4 million radar points [29]—a coverage of approximately 8.1 points per km^2. However, the data distribution is highly anisotropic, with high along-track point density (median spacing of 12.2 m), while lateral spacing between tracks is typically multiple kilometres. This can lead to relatively large differences between bed topographies generated using the different approaches described above (figure 2). A similar result is likely to be the case for generating synthetic bathymetries,

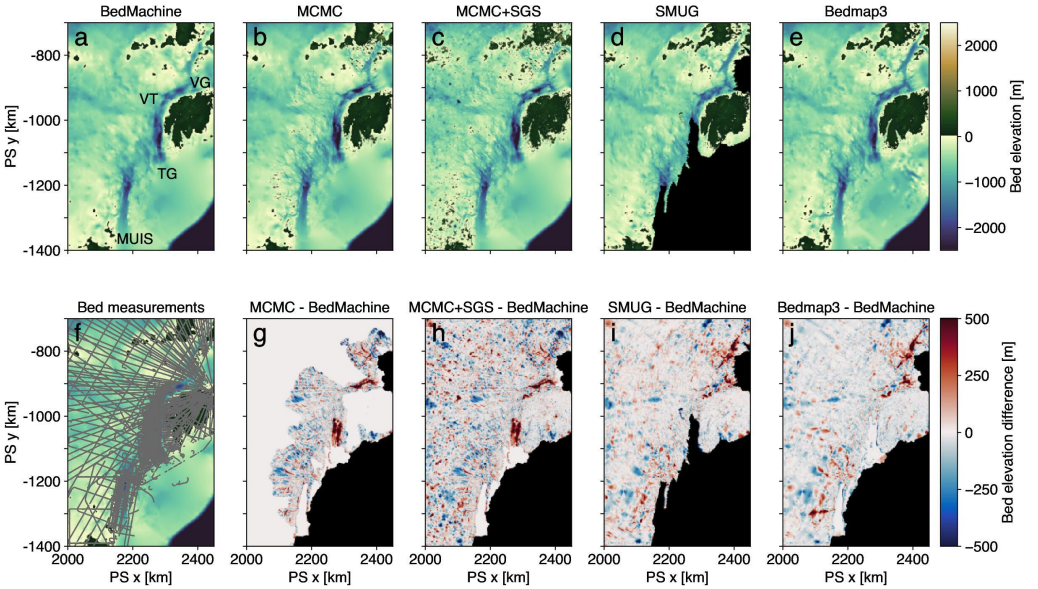

Figure 2. Bed elevation datasets (m) considered in our Aurora Subglacial Basin ensemble, zoomed into the Totten-MUIS region, as follows: (a) BedMachine [53]; (b) MCMC [73]; (c) MCMC with SGS conditioned based on MCMC (MCMC + SGS); (d) SMUG [46] and (e) Bedmap3 [44]. Locations of the Vanderford Trench (VT), Vanderford Glacier (VG), Totten Glacier (TG) and the Moscow University Ice Shelf (MUIS) are shown in panel (a). (f) Bed measurements from airborne radar surveys used in the generation of SMUG, Bedmap3 and the MCMC/MCMC + SGS bed topographies [28]. Differences between the BedMachine dataset and the MCMC, MCMC + SGS, SMUG and Bedmap3 datasets are shown in panels (g)–(j).

although their generation and corresponding implications for ocean modelling are not a focus of this study.

Here, we aim to better understand the impacts of the choice of bed topography on simulated sea-level rise and particularly examine where, and to what extent, evolution of the Aurora Subglacial Basin is sensitive to bed topography variations. To this end, we conduct ice sheet model simulations using an ensemble of bed topographies—comprising both elevation- and texture-preserving beds—forced using low and high emission scenarios to 2300 CE.

(a) Model and approach

(i) Model initialization

The ice sheet model domain is the Ice sheet Mass Balance Inter-comparison Exercise outline for the Aurora Subglacial Basin, East Antarctica [99], of which the key outlet glaciers are the Vanderford, Totten and Moscow University Ice Shelf (MUIS) Glaciers (e.g. [100]). The horizontal domain is partitioned into 416 515 triangular elements, with mesh refinement based on the MEaSUREs v. 2 ice velocities [101,102], with the horizontal element size increasing from approximately 500 m near the grounding line to a maximum of 40 km in the interior of the catchment. We use the BedMachine Antarctica v. 3 [54] dataset for initial bed and surface elevation, and grounded and floating ice masks to initialize the geometry, reinforcing hydrostatic equilibrium where interpolation errors onto the model mesh lead to floating ice geometry inconsistencies.

Inverse methods [60,103] and the Glen flow law [104–106], in conjunction with the MEaSUREs v. 2 ice surface velocity fields, are used to determine the ice rigidity on floating ice. We then use the Schoof friction law [107,108] to determine a basal friction coefficient over grounded ice via inversion, again with the MEaSUREs v. 2 ice surface velocity fields as the observational constraints.

To avoid spatial heterogeneities in the basal friction coefficient associated with the neglect of subglacial hydrological processes [90], which are known to be important in this region [19], we follow a similar set-up to that described in [21]. Specifically, we generate an effective pressure field from the GlaDS subglacial hydrology model implemented in ISSM (see also [22,23,109]) and use this field as input to the Schoof friction law. More details on the modelling procedure are provided in the electronic supplementary material, section S2. The resulting effective pressure field and the corresponding friction coefficient calculated using the BedMachine geometries are shown in the electronic supplementary material, figure S1, and are temporally invariant for each simulation.

(ii) Control simulation

Starting from the model initial state described above, we perform a 20 year relaxation simulation with a constant ice shelf basal melt rate [110], to ensure model fields are consistent (cf. [86]). Using the geometries and velocities at the end of the relaxation period, we simulate projections from 2015 to 2300 CE. We perform simulations under low and high emission scenarios using ocean thermal forcing and surface mass balance fields derived for the ISMIP6 Antarctic 2300 CE forcings [60,111]. For the low emission scenario, we use the NorESM1-M Representative Concentration Pathway (RCP) RCP2.6 scenario; for the high emission scenario, we use the UKESM1-0-LL Shared Socioeconomic Pathway (SSP) SSP5-8.5 scenario. In both cases, basal melt rates are calculated using the non-local quadratic ISMIP6 melt rate parametrization [112]. We note that the SSP5-8.5 scenario is generally considered to be a high-end, and less likely, scenario; however, in what follows, we focus mainly on the results from the high emission scenario because a stronger ice sheet response to increased ocean thermal forcing in this case should amplify differences between the simulations using different bed topographies, including any potential systematic differences between the beds generated using different methodologies. All prognostic simulations of the ice sheet model evolve the momentum and mass balance equations and grounding line location. A monthly model time step is used, and key model variables are output every model year. The calving front is kept fixed in all simulations.

(iii) Bed topography ensemble

We geostatistically simulate an ensemble of mass-conserving topographic realizations for the Aurora Subglacial Basin using a new MCMC approach [74]. This geostatistical inversion method iteratively perturbs geostatistical realizations of bed topography, using mass conservation as a constraint in fast-flowing regions (where surface velocities are greater than or equal to 50 m yr^{-1}), and accepting topographies based on the misfit in the ice flux using mass conservation and observed velocities. The geostatistical parameters that control the topography texture are calculated from the available radar-derived bed topography within the Aurora Subglacial Basin (within the high-velocity regions). Specifically, we calculated the variogram of the radar measurements and used the variogram parameters to specify the texture of the bed topography. When MCMC is used to generate each member in the topography ensemble, we ensure that the bed topography generated reconstructs the variogram. More details can be found in [74]. A total of five ensemble members were generated. To investigate the influence of bed variations distal to the grounding line where ice flow is too low to apply mass conservation constraints, we use an SGS, conditioned on one of the MCMC beds, to generate an additional 10 bed realizations (MCMC + SGS). The domain for the MCMC + SGS simulations is shown in figure 2; outside this domain, the bed topography is the BedMachine bed.

Using the final geometries and velocities from the relaxation simulation, we run prognostic simulations under the same ocean and atmosphere forcing described in §4a(ii) for each MCMC and MCMC + SGS bed realization, a bed realization generated using the SMUG algorithm [47], and the Bedmap3 bed topography [45]. For each bed realization, we run two simulations: one using the same basal friction coefficient as derived for the BedMachine configuration, and another

using basal friction coefficients generated from inversion for each bed realization under consideration. The histograms of the basal friction coefficients for the BedMachine simulation and each of the bed realizations are shown in the electronic supplementary material, figure S2, their differences in the electronic supplementary material, figure S3, and the Kolmogorov–Smirnov test statistic of significances in the differences between the friction field distributions, along with the corresponding p-values, are shown in the supporting electronic supplementary material, table S1.

Figure 2 compares the BedMachine bed with one realization of each of the MCMC and MCMC + SGS beds, and the SMUG and Bedmap3 beds for a subset of the Aurora Subglacial Basin, where the surface speed is greater than or equal to 50 m yr^{-1}. A few differences between the bed topographies are worth noting. First, the BedMachine bed is deeper than each of the other bed topographies in the Vanderford Trench within the region approximately 20–30 km upstream of the present-day Vanderford Glacier grounding line. Second, Bedmap3 is, on average, deeper than all other bed topographies upstream of the Vanderford Trench, although there are localized regions of higher elevation, and the SMUG and Bedmap3 datasets show the strongest agreement at the small scale (as might be expected, given both are generated using the same observational data [29]). As expected, the MCMC and MCMC + SGS bed topographies show much larger local deviations from BedMachine than both the SMUG and Bedmap3 bed topographies. The MCMC and MCMC + SGS realizations use the updated Totten bathymetry from [113], which was not incorporated in BedMachine v. 3, but does not impact our simulations, given we focus on scenarios likely to produce grounding line retreat, and the melt rate parametrization used does not depend on the ice shelf cavity geometry.

(b) Sensitivity of ice sheet evolution to ensemble-based projections

The retreat behaviour of the Aurora Subglacial Basin has been well documented in previous studies [4,60,114–116]. Here, we specifically consider the effect of different bed topography and friction coefficient realizations on the timing and rate of grounding line retreat.

Figure 3 shows the time series of the rate of change of ice mass above flotation (dM/dt, calculated by converting from ice volume above flotation to ice mass above flotation; left y-axis) and the corresponding global mean sea-level equivalent (right y-axis) for each bed realization. The evolution of both the grounding line location and ice thickness contributes to the change in ice mass above flotation in our simulations; here, we focus on describing the pattern in grounding line retreat, which evolves similarly in each simulation.

Glaciers in the Aurora Subglacial Basin show relatively linear and little retreat and mass loss under climate change to approximately 2115 CE under both RCP2.6 and SSPS5-8.5 scenarios (reflected in the smaller dM/dt values in figure 3). This trend persists throughout the simulation under RCP2.6 forcing. However, for the SSP5-8.5 scenario, from approximately 2115 to 2180 CE, grounding line retreat and mass loss accelerate rapidly. This is manifest in the merging of the grounding lines of the Totten, Vanderford and MUIS Glaciers, and the retreat to the southern edge of the Vanderford Trench—a topographic barrier to the inland Aurora Subglacial Basin. Ice mass loss continues beyond 2180 CE, with an increasing spread in the sea-level rise estimates, i.e. reflecting sensitivity to the bed topography and friction coefficient realization.

We observe a systematic difference in the magnitude of dM/dt and the sea-level equivalent between the BedMachine, SMUG and Bedmap3 topographies and the MCMC ensembles (figure 3; note that cumulative sea-level estimates are shown in the electronic supplementary material, figure S4). In particular, for the SSP5-8.5 scenario, the BedMachine, SMUG and Bedmap3 simulations generally reflect the greatest absolute rate of mass loss over the period of marked grounding line acceleration from 2115 to 2180 CE, and the largest sea-level rise by 2300 CE. By contrast, the MCMC ensembles—both MCMC and MCMC + SGS and for all friction coefficient realizations—have the lowest mass loss to 2300 CE. The result is similar for the RCP2.6 scenario, although the BedMachine topography initially shows mass loss rates consistent with the MCMC and MCMC + SGS topographies, before increasing from approximately 2200 CE in a similar pattern to the

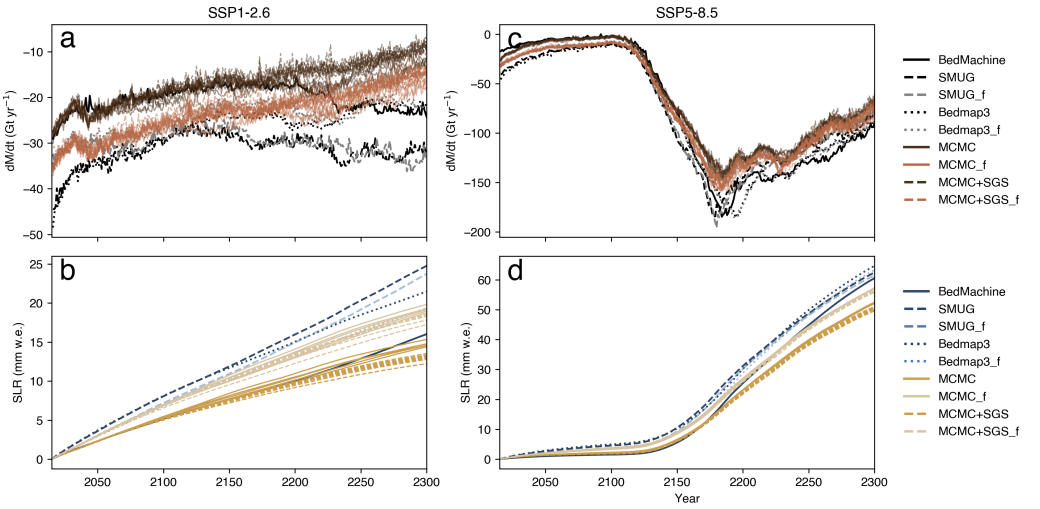

Figure 3. Simulations of the Aurora Subglacial Basin to 2300 CE. Rate of change of ice mass above flotation (d*M*/d*t*, Gt yr^{-1}) for the RCP2.6 scenario (a) and the SSP5-8.5 scenario (c); sea-level rise (SLR, mm water equivalent) for the RCP2.6 scenario (b) and the SSP5-8.5 scenario (d). The spread between the simulations that use the BedMachine Antarctica, SMUG, Bedmap3, MCMC and MCMC + SGS beds is shown for scenarios that use the friction coefficient derived from inversion using the BedMachine bed versus friction coefficients derived from inversion using each individual bed realization other than BedMachine (simulations with an _f suffix).

SMUG and Bedmap3 simulations. Given that the simulations start from a different initial ice volume (due to differences in the bed topography and hence ice thickness; although the maximum difference in initial ice mass above flotation is 0.36%), it is not unexpected that the initial d*M*/d*t* values vary accordingly. Despite these variations in d*M*/d*t* magnitude, the overall shape of d*M*/d*t* for all simulations is very similar, which highlights the importance of the large horizontal-scale bed variations in determining the overall behaviour in the grounding line evolution of this region.

As expected, the d*M*/d*t* and sea-level contributions reflect differences in both the bed topographies and the basal friction coefficients. Generally, the simulations that use the same friction coefficient as BedMachine show a much larger spread, equating to a greater systematic difference in final sea-level contributions (this equates to the smallest sea-level equivalent being approx. 23% less than the largest across all ensemble members at 2300 CE for the SSP5-8.5 scenario and 51% for the RCP2.6 scenario) than the simulations with friction coefficients optimized for each bed realization (approx. 11% for SSP5-8.5 and 32% for RCP2.6). The difference between sea-level contributions in the MCMC members that use the two different friction coefficient approaches is generally larger than the spread between individual members of each set. The electronic supplementary material, figure S2, shows histograms of friction coefficients for each bed realization, and the electronic supplementary material, figure S3, shows differences between the friction coefficients generated using BedMachine and each of the MCMC, MCMC + SGS, SMUG and Bedmap3 bed topographies. We note that the differences in the distributions of friction coefficients are not statistically significantly different between any ensemble member compared with the BedMachine friction coefficient (electronic supplementary material, table S1). Rather, the differences between the friction coefficients are attributable to local-scale shifts in extrema corresponding to local-scale bed topography fluctuations between each bed realization. This is particularly important in the region close to the grounding line, where small differences in the friction coefficient can lead to a markedly different timing in the onset of grounding line retreat.

Next, we examine the differences in the evolution of the grounding line location as a function of variations in bed topography and basal friction coefficient, focusing on the SSP5-8.5 scenario. Figure 4 shows the grounding line evolution along six streamlines calculated using the MEaSUREs

v. 2 ice surface velocity fields, focused on the Totten and MUIS Glaciers. For simplicity, in figure 4 we show only the results that use the same friction coefficient realization (derived from inversion using the BedMachine bed), comparing results for BedMachine, SMUG, Bedmap3 and one MCMC realization. The full set of comparisons is shown in the electronic supplementary material, figure S5. All beds generally capture the same large horizontal-scale variations, with greater vertical differences at finer horizontal scales. This is particularly notable for profiles 3 and 4, where local vertical differences between the BedMachine and MCMC beds can be greater than 200 m across horizontal scales of 2–5 km. Large vertical differences in the bed do not necessarily always translate to large differences in the evolution of the grounding line retreat, except where they influence: (i) the timing of the onset of grounding line retreat, and (ii) the final grounding line position. For example, there is relatively little difference in the grounding line evolution of profiles 1 and 2: grounding line retreat initiates at a similar year, the rate of retreat is very consistent between different ensemble members, and the final grounding line position is very similar. For profile 3, the BedMachine, SMUG and Bedmap3 grounding line retreat is delayed by 50–100 years compared with the MCMC ensemble; once initiated, grounding line retreat occurs very similarly for all bed topographies. For profile 4, again, the grounding line retreat rate is similar across simulations, except in the final approximately 100 years, where the BedMachine, SMUG and Bedmap3 simulations show approximately 25 km more grounding line retreat than the MCMC ensemble, most likely linked to larger systematic differences between these bed elevation realizations compared with the MCMC ensemble members. For profiles 5 and 6, the timing of the onset of retreat and the final grounding line positions vary more considerably, again as a function of variations in the bed, with the MCMC bed showing earlier retreat onset. As expected (given the dM/dt and sea-level results in figure 3), the differences across the MCMC and MCMC + SGS ensemble members are generally smaller than the differences between the MCMC and MCMC + SGS ensembles and the BedMachine, SMUG and Bedmap3 realizations (electronic supplementary material, figure S5).

5. Discussion

(a) The utility of synthetic bed topographies

We first revisit the utility of synthetic bed topographies in light of their underlying design objectives: namely, whether they preserve elevation (BedMachine, SMUG, Bedmap3) or texture (MCMC, MCMC + SGS). As discussed in §2, elevation-preserving datasets aim to realistically represent the large-scale shape and gradients in the bed, and therefore might produce a more realistic response in ice sheet models where the data density is sufficiently high to constrain key bed features. However, the key question here is, what is dense enough? A previous study [1] demonstrated that, to constrain sea-level rise uncertainty within ±20 cm from Thwaites Glacier, bed observations must be spaced at least every 2 km horizontally, with a vertical accuracy of at least 8 m. No such density in radar surveys exists at the catchment scale, particularly within critical regions likely to contribute to sea-level rise over the coming centuries [59,60]. Ensemble approaches based on elevation-preserving bed topographies (e.g. [1,91]) can provide insight into the effects of the bed uncertainty on the ice sheet evolution, but the representativeness of simulated landform amplitude and wavelength—and the ability of such datasets to capture the character of pinning points—remains a central challenge.

By contrast, texture-preserving topographies, such as the MCMC and MCMC + SGS realizations examined here, aim to reproduce the statistical structure of surveyed landforms, including the amplitude and periodicity of bed undulations observed in radar data. These datasets are designed to replicate the morphology of landforms, such as subglacial ridges, troughs and rough patches, even where observations are sparse. By preserving textural properties, they may offer an improved representation of the characteristics of likely pinning points and other features, specific to the region of interest, and which are crucial for simulations of grounding line retreat. While such datasets may sacrifice small-scale elevation accuracy, their ability to realistically

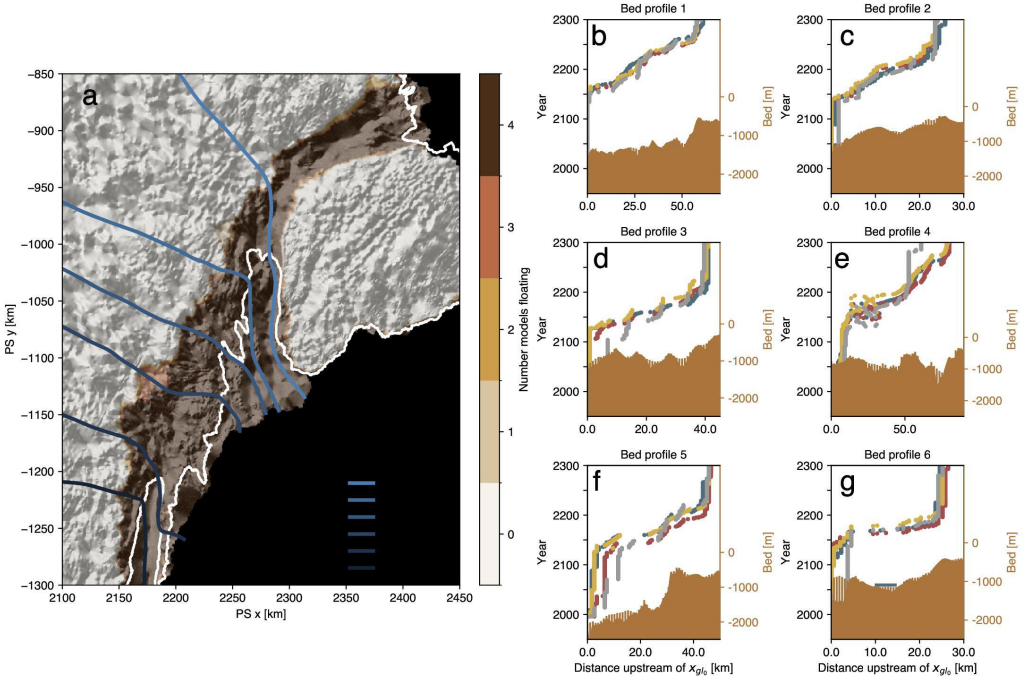

Figure 4. (a) Shading shows the number of ensemble members that predict floating ice in the region of the Totten and MUIS Glaciers on a background hillshade model of BedMachine v. 3 Antarctica, with the white line designating the present-day grounding line position [53]. Six streamlines are shown (blue lines), which correspond to the profiles in panels (b)–(g). The median of the BedMachine, SMUG, Bedmap3, MCMC and MCMC + SGS beds is shown (solid brown line; right *y*-axis), with the range (minimum to maximum of all bed realizations) indicated by vertical lines. The grounding line retreat over time for the BedMachine, SMUG, Bedmap3 and one MCMC bed realization is shown in coloured dotted lines (left *y*-axis). The profiles for the simulations using all scenarios are shown in the electronic supplementary material, figure S5.

sample the range of bed geometries expected in Antarctic catchments is valuable for robust uncertainty quantification in ice sheet models, particularly in regions where data are sparse. Ultimately, texture-preserving topographies can complement elevation-preserving approaches by capturing unsampled fine-scale bed features that may strongly control ice dynamics.

A key element of all the bed datasets discussed in this study is their estimate of uncertainty. Robust uncertainty estimates of bed topography are critical because they define the limits of what can be inferred, both about a given bed topography dataset and the ice sheet model experimental design. Uncertainties comprise observational, intra- and inter-algorithm differences, and the method of interpolation onto ice sheet model grids (which is a function of the model resolution), and can directly influence ice sheet dynamics, including through parameters like the basal friction coefficient. Furthermore, when uncertainties are robustly quantified (as for the SMUG and MCMC algorithms considered in this paper), they can be used in ice sheet model simulations (including, e.g. through analyses such as the DAKOTA framework [33,34]), and the results can be used to inform experimental design, model sensitivity studies and future airborne radar surveys targeting observations of the ice–bed interface.

In §5b below, we discuss implications of our case study focused on how different bed topographies, including both elevation- and texture-preserving beds, impact ice sheet evolution and associated sea-level contributions from the Aurora Subglacial Basin, East Antarctica. While this provides important insight into one key impact of bed uncertainties—i.e. sea-level rise—bed topography also influences other processes at the ice–bed interface, including heat transfer, which impact the basal ice temperature, basal melt rates, sliding and subglacial hydrology. We discuss these in more detail in §5c.

(b) Ice sheet sensitivity to bed topography in the Aurora Subglacial Basin

A key aim of our study was to investigate ice sheet sensitivity to bed variations. We did this using an ensemble ice sheet modelling approach with realizations of bed topography generated using different methodologies, including those that preserve elevation and those that preserve texture.

Overall, we find that small differences in the bed topography (and friction coefficient, as discussed in more detail in §5c) can significantly impact ice sheet evolution in the Aurora Subglacial Basin under both low and high emission scenarios. In particular, for the SSP5-8.5 scenario, the timing of the onset of rapid grounding line retreat locally varies by up to approximately 100 years depending on the bed topography realization. We highlight *local* here, given that while all bed realizations similarly captured the large-scale bed features of the region, it was local differences in key regions—close to the present-day grounding line and the upstream edge of the Vanderford Trench—that led to the marked differences in the timing of the onset of rapid retreat and in the final grounding line position (e.g. [2,5]). This highlights the urgent need for targeted radar surveys to constrain the bed topography directly upstream of the present-day grounding line and within the region of likely grounding line retreat over the coming decades to centuries.

Despite local vertical differences in bed topography realizations of over 200 m, the rate of retreat, once initiated, was relatively insensitive to the bed elevation. That is, all our simulations showed very consistent retreat rates for both optimized and non-optimized friction coefficients [117]. This could be partly related to the particulars of this system. That is, the retreat of the Totten and Vanderford Glaciers through the deeply incised Vanderford Trench and between the eastern flank of the Totten and MUIS Glaciers is rapid once initiated, a finding that is also supported by the inferred geomorphology of the basin [114]. This behaviour is consistent with the region's marine-based bed and vulnerability to a warming ocean.

Given that we did not use automatic differentiation in this study, we cannot say from our experiments where the system is most sensitive to uncertainties in the bed topography—i.e. how the magnitude versus the location of bed variations impact the system. Nevertheless, given that the MCMC beds vary from the BedMachine bed topography only within the 50–100 km upstream of the present-day grounding line, our simulations reflect high sensitivity to bed topography near the grounding line, which is consistent with previous studies (e.g. [1,91]). Interestingly, the MCMC + SGS simulations (although all conditioned on one realization of MCMC) show consistently less sea-level contributions than any of the MCMC simulations, which is evidence that distal bed topography can influence ice mass loss; however, this effect is secondary compared with the effects of differences close to the grounding line.

Finally, we observe a systematic difference in the sea-level projections derived from the elevation- and texture-preserving bed realizations analysed here, particularly for the SSP5-8.5 scenario. Given the relatively small sample size of the MCMC and MCMC + SGS ensembles, we cannot determine whether this result can be generalized to all plausible bed topographies within the two different categories (i.e. bed topographies that also meet the mass-conserving constraint). We generally find that the large-scale topographies (lateral dimension greater than approx. 10–20 km) in the MCMC ensembles are very similar. Hence, if the large-scale topography is the greatest factor in determining the differences between the results using the MCMC ensembles and the other topographies, then increasing the MCMC ensemble size is unlikely to change our results. If, by contrast, finer scale topography dominates the differences, as found in other studies (e.g. [1]), then it is quite likely that our result of systematic differences between the MCMC ensemble members and the other topographies is robust, given the relative lack of fine-scale variation in the BedMachine, Bedmap3 and SMUG topographies, and that we expect the differences between the MCMC ensemble members and the other topographies to be larger than the differences within the MCMC ensemble members. Overall, this emphasizes the important role of fine-scale bed variability introduced through preserving texture.

The systematic differences between the sea-level projections for the different bed topographies broadly hold for both SSP5-8.5 and RCP2.6 emission scenarios. Two notable differences arise between the results from these emission scenarios. First, there is a greater spread (approximately

a factor of 2) in the 2300 CE sea-level rise projections in the RCP2.6 scenario compared with the SSP5-8.5 scenario. We attribute this to a lower magnitude ocean thermal forcing in the RCP2.6 scenario that leads to lower absolute rates of mass loss compared with the SSP5-8.5 scenario (figure 3). Second, the BedMachine projection of sea-level rise is within the spread of the MCMC and MCMC + SGS ensemble in the RCP2.6 scenario, in contrast to the SMUG and Bedmap3 projections. This reflects generally lower absolute rates of mass loss using the BedMachine than using SMUG and Bedmap3 bed topographies in the first approximately 175 years, although the BedMachine dM/dt time series more closely matches the SMUG and Bedmap3 time series than those that use the MCMC and MCMC + SGS beds. By approximately 2200 CE, the absolute mass loss rates in BedMachine increase in magnitude more substantially than the MCMC and MCMC + SGS simulations, and the sea-level rise increases at a faster rate (although we note that the cumulative sea-level rise at 2300 CE in BedMachine is more consistent with the MCMC ensemble members under both RCP2.6 and SSP5-8.5 scenarios, reflecting the lower initial mass loss using the BedMachine topography; electronic supplementary material, figure S4). We expect that if we had continued the forcing beyond 2300 CE, we would eventually see that the BedMachine, SMUG and Bedmap3 bed topographies produce higher sea-level rise than the MCMC and MCMC + SGS scenarios, and a similar systematic difference between bed topographies generated using the two different methodologies (i.e. texture versus elevation preserving).

The SMUG, Bedmap3 and MCMC datasets of bed topography over the grounded ice sheet—relevant to our simulations of grounding line retreat to 2300 CE—were all generated using the same underlying input data (i.e. [29]). Although BedMachine v. 3 does not include the updates from [29], the limited additional data from new surveys in the Aurora Subglacial Basin are unlikely to substantially change the BedMachine bed topography for this region. Furthermore, the differences between the BedMachine and MCMC beds are not systematically larger than the differences between either the Bedmap3 or SMUG beds and the MCMC beds, which strengthens our confidence that the systematic differences in the MCMC-derived sea-level estimates are not due to discrepancies in input bed topography data. Rather, the differences may stem from differences in the structural and statistical approaches used to generate the MCMC ensemble compared with the other datasets, including, e.g. the 'roughness' of the MCMC beds compared with the other beds and the effect of the texture on the simulated buttressing. The relatively small size of the MCMC bed ensemble means it may not fully capture the broader uncertainty space associated with that method, and further bed realizations may be needed to assess whether the observed differences are representative or a result of a too-small sample size. Our preliminary findings suggest that methodological choices—such as how bed topography variability and uncertainty are represented, even if the differences are localized—can have a significant impact on derived sea-level estimates. This highlights the importance of using bed ensembles and how the design objectives for generating bed topographies may influence the kinds of questions they can be used to address.

(c) Looking forward: constraining properties and processes at the ice–bed interface

In this study, we focused on the sensitivity of projected sea-level rise to variations in bed topography and friction coefficient. When the basal friction coefficient was optimized individually for each bed topography, differences in projected SLR to 2300 CE were smaller (maximum difference of 11% at 2300 CE under the SSP5-8.5 scenario and 32% for RCP2.6). However, a larger spread (up to 23% at 2300 CE under the SSP5-8.5 scenario and 51% for RCP2.6) emerged when a constant friction coefficient was imposed across all ensemble members, with particularly divergent sea-level contributions over time (see also the electronic supplementary material, figure S4). This result is expected, given that the non-optimized basal friction fields were inconsistent with all but the BedMachine ice sheet initial state (e.g. geometry, velocities), which can shock the system into a more rapid onset of retreat. That is, the power of data assimilation approaches, like the inverse method employed here, is that they optimize the friction coefficient for the particular

model fields—the surface velocity and ice geometry—and hence better capture the ice sheet state at a snapshot in time [118]. Recent developments have incorporated transient data assimilation so that trends (e.g. in ice thickness) are also accurately represented [119] on decadal timescales. However, inverse methods achieve that at the potential risk of overfitting [120,121], such that relatively small differences in the friction coefficient arising from inconsistencies between input fields can lead to relatively large differences in sea-level rise, as we found here. Indeed, the median of the maximum percentage difference between the BedMachine friction coefficient and each of the 17 other optimized friction coefficient fields is 1.34% (minimum 0.95%; maximum 8.09%). The effects of this, and of prescribing temporally constant basal friction coefficients, on the long-term evolution of the ice sheet remain open questions. It follows that understanding the processes that influence basal friction and how they are represented in ice sheet models is essential for developing physically informed parametrizations that complement and strengthen data assimilation approaches. Here, we discuss a number of properties and processes at the ice–bed interface that are relevant to consider in improving the representation of basal friction.

Basal friction is influenced by several related factors, including: (i) bed topography, which influences form drag directly as ice flows over topography, and skin drag indirectly through modulation of the subglacial hydrology and local frictional forces (e.g. [122]); (ii) geological substrate, which influences the relative contributions of hard-bedded sliding versus bed deformation [106,121,123]; (iii) subglacial hydrology, particularly the presence of an inefficient/distributed drainage system, which strongly controls the effective pressure at the bed [19–21]; and (iv) heat sources at the bed, including geothermal, frictional and deformational heating, which together influence basal meltwater production [124] and the temperature, and hence viscosity, of the basal ice [17,18]. The above factors are strongly interdependent and are modulated by the bed topography, through its influence on drag, and both frictional and deformational heat production at the ice base. For example, bed roughness can lead to the formation of basal temperate layers through increases in local shear deformation relative to a smoother realization of the bed, with implications for the balance between ice flow processes [14]. Topography further affects the direction and concentration of geothermal heat flow to the basal ice layers: depending on the shape and thermal conductivity of the subglacial material, geothermal heat can funnel heat into valleys and depressions where thermal gradients and conductivity are highest or to ridges where the ice has lower thermal conductivity [28,125].

Topography and the permeability of the bed substrate also control the nature of the subglacial hydrological system. Rough topography promotes variable water flow pathways [42], influencing basal sliding and the redistribution of heat by basal water [126]. Topographic depressions can act as thermal water reservoirs, where latent heat exchange through freeze-melt cycles regulates basal temperatures [127]. The geological substrate also influences whether efficient or inefficient drainage systems are supported, which, in turn, shapes the basal friction and flow regime, and the relative contributions of sliding versus deformational flow [16].

These coupled processes feed back into sea-level projections via their influence on grounding line dynamics. Several ice sheet modelling studies have investigated the effects of some of these feedbacks (including e.g. [22,23]), and some ice sheet models explicitly parametrize processes in the till (e.g. [128]). However, work still remains to better understand interactions between ice thermo-mechanical, subglacial hydrological and geological systems, the timescales over which they are relevant and how they can be better represented in ice sheet models.

6. Conclusion

This study examined the utility of bed topographies generated with different objectives—namely, elevation- versus texture-preserving beds—and corresponding differences in basal friction coefficients, on ice sheet model simulations of sea-level rise in the Aurora Subglacial Basin, East Antarctica. While we identified systematic differences between the sea levels predicted using bed realizations generated to preserve elevation versus texture, the relatively small size of the MCMC

ensemble limits our ability to explore the full plausible sea-level range for the texture-preserving beds. Expanding MCMC ensembles will be needed to fully characterize uncertainties and understand the implications of differing objectives for synthetic bed topography generation. Our results point to the importance of constraining realism in bed topography datasets and the value of targeted surveys focused on regions directly upstream of marine grounding lines, where bed uncertainty has the greatest impact on ice sheet-driven sea-level rise. Finally, our simulations highlight the critical role of the basal friction coefficient in shaping ice sheet evolution, whereby small, localized variations in the basal friction field can lead to large differences in the timing of grounding line retreat and ultimate sea-level contributions. Given that the basal friction fields we generated were optimized for ice sheet geometry at a particular snapshot in time, this has implications for the applicability of such fields for long-term ice sheet projections. We advocate for the development of process-based representations of basal friction for ice sheet modelling, which capture relevant ice-bed properties and transient processes realistically and ideally at low computational cost.

Data accessibility. Scalar outputs derived from two-dimensional ice sheet modelling fields, bed topography datasets and the routines used for data analysis and figure generation are available at Zenodo:10.5281/zenodo.17176762. We use v. 4.24 of the open-source ISSM software, which is freely available for download from https://github.com/ISSMteam/ISSM. The datasets used to initialize the model are available via the corresponding articles cited in this paper.

Supplementary material is available online [129].

Declaration of AI use. We have used AI-assisted technologies in creating this article. AI-assisted technologies were used in debugging and improving the readability of numerical code (Python) used for the data analysis and visualization in this study.

Authors' contributions. F.S.M.: conceptualization, data curation, formal analysis, investigation, methodology, project administration, resources, supervision, validation, visualization, writing—original draft, writing— review and editing; T.S.: conceptualization, visualization, writing—original draft, writing—review and editing; N.S.: data curation, formal analysis, writing—original draft, writing—review and editing; E.M.: conceptualization, writing—original draft, writing—review and editing; A.F.H.: writing—original draft, writing—review and editing; M.L.: writing—original draft, writing—review and editing; J.R.: conceptualization, writing—original draft, writing—review and editing; S.E.: writing—original draft, writing—review and editing; C.D.: writing—original draft, writing—review and editing.

All authors gave final approval for publication and agreed to be held accountable for the work performed therein.

Conflict of interest declaration. We declare we have no competing interests.

Funding. This research was supported by the Australian Research Council (ARC) Special Research Initiative (SRI) Securing Antarctica's Environmental Future (SR200100005), the ARC Discovery Early Career Award (DE210101433), ARC Discovery Project (DP190100418), the ARC Special Research Initiative Australian Centre for Excellence in Antarctic Science (SR200100008) and in part by grant NSF PHY-2309135 to the Kavli Institute for Theoretical Physics (KITP).

Acknowledgements. F.S.M. benefited from insightful discussions with Mathieu Morlighem and Frank Pattyn on topics explored in this research. C.D. was supported by the Natural Sciences and Engineering Research Council of Canada (NSERC RGPIN-03761-2017) and the Canada Research Chairs Program (CRC 950-231237). This paper is a contribution to Australian Antarctic Science projects 4077, 4346 and 4511 and contributes to delivering the Australian Antarctic Science Decadal Strategy.

References

1. Castleman BA, Schlegel NJ, Caron L, Larour E, Khazendar A. 2022 Derivation of bedrock topography measurement requirements for the reduction of uncertainty in ice-sheet model projections of Thwaites Glacier. *The Cryosphere* **16**, 761–778. (doi:10.5194/tc-16-761-2022)
2. Houriez L *et al*. 2025 Reinforced ridges in Thwaites Glacier yield insights into resolution requirements for coupled ice sheet and solid Earth models. *The Cryosphere* **19**, 4355–4372. (doi: 10.5194/tc-19-4355-2025)

3. McCormack FS, Roberts JL, Gwyther DE, Morlighem M, Pelle T, Galton-Fenzi BK. 2021 The impact of variable ocean temperatures on Totten Glacier stability and discharge. *Geophys. Res. Lett*. **48**, e2020GL091790. (doi:10.1029/2020GL091790)
4. Robel AA, Pegler SS, Catania G, Felikson D, Simkins LM. 2022 Ambiguous stability of glaciers at bed peaks. *J. Glaciol*. **68**, 1177–1184. (doi:10.1017/jog.2022.31)
5. Roberts JL *et al*. 2018 Ocean forced variability of Totten Glacier mass loss. In *Geological society*, pp. 175–186, vol. **461**. London, UK: Special Publications. (doi:10.1144/SP461.6)
6. Schoof C. 2007 Marine ice-sheet dynamics. Part 1. The case of rapid sliding. *J. Fluid Mech*. **573**, 27–55. (doi:10.1017/S0022112006003570)
7. Schoof C. 2012 Marine ice sheet stability. *J. Fluid Mech*. **698**, 62–72. (doi:10.1017/jfm.2012.43)
8. Sergienko OV, Wingham DJ. 2022 Bed topography and marine ice-sheet stability. *J. Glaciol*. **68**, 124–138. (doi:10.1017/jog.2021.79)
9. Weertman J. 1974 Stability of the junction of an ice sheet and an ice shelf. *J. Glaciol*. **13**, 3–11. (doi:10.1017/S0022143000023327)
10. Matsuoka K *et al*. 2015 Antarctic ice rises and rumples: their properties and significance for ice-sheet dynamics and evolution. *Earth Sci. Rev*. **150**, 724–745. (doi:10.1016/j.earscirev.2015.09.004)
11. Gudmundsson GH, Paolo FS, Adusumilli S, Fricker HA. 2019 Instantaneous Antarctic ice sheet mass loss driven by thinning ice shelves. *Geophys. Res. Lett*. **46**, 13903–13909. (doi:10.1029/2019GL085027)
12. Reese R, Gudmundsson GH, Levermann A, Winkelmann R. 2018 The far reach of ice-shelf thinning in Antarctica. *Nat. Clim. Chang*. **8**, 53–57. (doi:10.1038/s41558-017-0020-x)
13. Law R, Christoffersen P, MacKie E, Cook S, Haseloff M, Gagliardini O. 2023 Complex motion of Greenland Ice Sheet outlet glaciers with basal temperate ice. *Sci. Adv*. **9**, eabq5180. (doi:10.1126/sciadv.abq5180)
14. Law R, ChandlerD, Born A. 2025 What is glacier sliding? (doi:10.48550/arXiv.2407.13577)
15. McCormack FS, Warner RC, Seroussi H, Dow CF, Roberts JL, Treverrow A. 2022 Modeling the deformation regime of Thwaites Glacier, West Antarctica, using a simple flow relation for ice anisotropy (ESTAR). *J. Geophys. Res*. **127**, e2021JF006332. (doi:10.1029/2021JF006332)
16. Pattyn F. 2010 Antarctic subglacial conditions inferred from a hybrid ice sheet/ice stream model. *Earth Planet. Sci. Lett*. **295**, 451–461. (doi:10.1016/j.epsl.2010.04.025)
17. Raspoet O, Pattyn F. 2025 Estimates of basal and englacial thermal conditions of the Antarctic ice sheet. *J. Glaciol*. **71**, 1–39. (doi:10.1017/jog.2025.10087)
18. Dow CF, McCormack FS, Young DA, Greenbaum JS, Roberts JL, Blankenship DD. 2020 Totten Glacier subglacial hydrology determined from geophysics and modeling. *Earth Planet. Sci. Lett*. **531**, 115961. (doi:10.1016/j.epsl.2019.115961)
19. Dow CF, Ross N, Jeofry H, Siu K, Siegert MJ. 2022 Antarctic basal environment shaped by high-pressure flow through a subglacial river system. *Nat. Geosci*. **15**, 892–898. (doi:10.1038/s41561-022-01059-1)
20. Ehrenfeucht S, Dow C, McArthur K, Morlighem M, McCormack FS. 2025 Antarctic wide subglacial hydrology modeling. *Geophys. Res. Lett*. **52**, e2024GL111386. (doi:10.1029/2024GL111386)
21. Pelle T, Greenbaum JS, Dow CF, Jenkins A, Morlighem M. 2023 Subglacial discharge accelerates future retreat of Denman and Scott Glaciers, East Antarctica. *Sci. Adv*. **9**, eadi9014. (doi:10.1126/sciadv.adi9014)
22. Pelle T, Greenbaum JS, Ehrenfeucht S, Dow CF, McCormack FS. 2024 Subglacial discharge accelerates dynamic retreat of aurora subglacial basin outlet glaciers, East Antarctica, over the 21st century. *J. Geophys. Res*. **129**, e2023JF007513. (doi:10.1029/2023JF007513)
23. Greenbaum JS *et al*. 2015 Ocean access to a cavity beneath Totten Glacier in East Antarctica. *Nat. Geosci*. **8**, 294–298. (doi:10.1038/ngeo2388)
24. Goldberg DN, Smith TA, Narayanan SHK, Heimbach P, Morlighem M. 2020 Bathymetric influences on Antarctic ice-shelf melt rates. *J. Geophys. Res*. **125**, e2020JC016370. (doi:10.1029/2020JC016370)
25. Haigh M, Holland PR, Jenkins A. 2023 The influence of bathymetry over heat transport onto the amundsen sea continental shelf. *J. Geophys. Res*. **128**, e2022JC019460. (doi:10.1029/2022JC019460)

26. Colgan W, MacGregor JA, Mankoff KD, Haagenson R, Rajaram H, Martos YM, Morlighem M, Fahnestock MA, Kjeldsen KK. 2021 Topographic correction of geothermal heat flux in Greenland and Antarctica. *J. Geophys. Res*. **126**, e2020JF005598. (doi:10.1029/2020JF005598)
27. Willcocks S, Hasterok D, Jennings S. 2021 Thermal refraction: implications for subglacial heat flux. *J. Glaciol*. **67**, 875–884. (doi:10.1017/jog.2021.38)
28. Frémand AC *et al*. 2023 Antarctic bedmap data: findable, accessible, interoperable, and reusable (FAIR) sharing of 60 years of ice bed, surface, and thickness data. *Earth Syst. Sci. Data* **15**, 2695–2710. (doi:10.5194/essd-15-2695-2023)
29. Clyne ER, Anandakrishnan S, Muto A, Alley RB, Voigt DE. 2020 Interpretation of topography and bed properties beneath Thwaites Glacier, West Antarctica using seismic reflection methods. *Earth Planet. Sci. Lett*. **550**, 116543. (doi:10.1016/j.epsl.2020.116543)
30. Tsutaki S *et al*. 2022 High-resolution subglacial topography around Dome Fuji, Antarctica, based on ground-based radar surveys over 30 years. *The Cryosphere* **16**, 2967–2983. (doi:10.5194/tc-16-2967-2022)
31. Matsuoka K *et al*. 2025 Towards an improved understanding of the Antarctic coastal zone and its contribution to future global sea level. *ESS Open Archive*. (doi:10.22541/essoar.175241971.19851046/v1)
32. Larour E, Schiermeier J, Rignot E, Seroussi H, Morlighem M, Paden J. 2012 Sensitivity analysis of Pine Island Glacier ice flow using ISSM and DAKOTA. *J. Geophys. Res*. **117**, 1–16. (doi:10.1029/2011JF002146)
33. Schlegel NJ, Seroussi H, Schodlok MP, Larour EY, Boening C, Limonadi D, Watkins MM, Morlighem M, van den Broeke MR. 2018 Exploration of Antarctic Ice Sheet 100-year contribution to sea level rise and associated model uncertainties using the ISSM framework. *The Cryosphere* **12**, 3511–3534. (doi:10.5194/tc-12-3511-2018)
34. Seroussi H, Morlighem M, Rignot E, Larour E, Aubry D, Ben Dhia H, Kristensen SS. 2011 Ice flux divergence anomalies on 79north Glacier, Greenland. *Geophys. Res. Lett*. **38**, 1–5. (doi:10.1029/2011GL047338)
35. Dorschel B *et al*. 2022 The international bathymetric chart of the Southern Ocean version 2. *Sci. Data* **9**, 275. (doi:10.1038/s41597-022-01366-7)
36. Bird LA *et al*. 2025 Gravity-derived Antarctic bathymetry using the Tomofast-x open-source code: a case study of Vincennes Bay. *The Cryosphere* **19**, 3355–3380. (doi:10.5194/tc-19-3355-2025)
37. Charrassin R, Millan R, Rignot E, Scheinert M. 2025 Bathymetry of the Antarctic continental shelf and ice shelf cavities from circumpolar gravity anomalies and other data. *Sci. Rep*. **15**, 1214. (doi:10.1038/s41598-024-81599-1)
38. Scheinert M *et al*. 2016 New Antarctic gravity anomaly grid for enhanced geodetic and geophysical studies in Antarctica. *Geophys. Res. Lett*. **43**, 600–610. (doi:10.1002/2015GL067439)
39. Scheinert M, Zingerle P, Schaller T, Pail R, Willberg M. 2021 Towards an updated, enhanced regional gravity field solution for Antarctica. In vEGU21, the 23rd EGU General Assembly, held online 19–30 April, ID, EGU21-9873EGU General Assembly Conference Abstracts. (doi:10.5194/egusphere-egu21-9873)
40. MacKie EJ, Schroeder DM. 2020 Geostatistically simulating subglacial topography with synthetic training data. In *IGARSS 2020 - 2020 IEEE International Geoscience and Remote Sensing Symposium*, Waikoloa, HI, pp. 2991–2994. IEEE. (doi:10.1109/IGARSS39084.2020.9324563). https://ieeexplore.ieee.org/xpl/mostRecentIssue.jsp?punumber=9323073.
41. MacKie EJ, Field M, Wang L, Yin Z, Schoedl N, Hibbs M, Zhang A. 2023 GStatSim V1.0: a python package for geostatistical interpolation and conditional simulation. *Geosci. Model Dev*. **16**, 3765–3783. (doi:10.5194/gmd-16-3765-2023)
42. Lythe MB, Vaughan DG. 2001 BEDMAP: a new ice thickness and subglacial topographic model of Antarctica. *J. Geophys. Res*. **106**, 11335–11351. (doi:10.1029/2000JB900449)
43. Fretwell P *et al*. 2013 Bedmap2: improved ice bed, surface and thickness datasets for Antarctica. *The Cryosphere* **7**, 375–393. (doi:10.5194/tc-7-375-2013)
44. Pritchard HD *et al*. 2025 Bedmap3 updated ice bed, surface and thickness gridded datasets for Antarctica. *Sci. Data* **12**, 414. (doi:10.1038/s41597-025-04672-y)
45. Hutchinson MF. 1989 A new procedure for gridding elevation and stream line data with automatic removal of spurious pits. *J. Hydrol.* **106**, 211–232. (doi:10.1016/0022-1694(89)90073-5)

46. Jong LM, Roberts JL, McCormackFS, Fabela Hinojosa A. 2025 Antarctic bed topography estimation using a stochastic meshless uncertainty gridding (SMUG) method. *In preparation*
47. Roberts JL. 2024 Meshless weighting coefficients for arbitrary nodes: the efficient computation to machine precision using hyper-dual numbers. *Adv. Eng. Softw*. **197**, 103753. (doi:10.1016/j.advengsoft.2024.103753)
48. Budd WF. 1970 Ice flow over bedrock perturbations. *J. Glaciol*. **9**, 29–48. (doi:10.3189/S0022143000026770)
49. Gudmundsson GH. 2003 Transmission of basal variability to a glacier surface. *J. Geophys. Res*. **108**. (doi:10.1029/2002JB002107)
50. Ockenden H, Bingham RG, Curtis A, Goldberg D. 2022 Inverting ice surface elevation and velocity for bed topography and slipperiness beneath Thwaites Glacier. *The Cryosphere* **16**, 3867–3887. (doi:10.5194/tc-16-3867-2022)
51. Ockenden H, Bingham RG, Curtis A, Goldberg D. 2023 Ice-flow perturbation analysis: a method to estimate ice-sheet bed topography and conditions from surface datasets. *J. Glaciol*. **69**, 1677–1686. (doi:10.1017/jog.2023.50)
52. Morlighem M *et al*. 2017 BedMachine v3: complete bed topography and ocean bathymetry mapping of Greenland from multibeam echo sounding combined with mass conservation. *Geophys. Res. Lett*. **44**, 11051–11061. (doi:10.1002/2017GL074954)
53. Morlighem M *et al*. 2020 Deep glacial troughs and stabilizing ridges unveiled beneath the margins of the Antarctic ice sheet. *Nat. Geosci*. **13**, 132–137. (doi:10.1038/s41561-019-0510-8)
54. Morlighem M, RignotE, Mouginot J, Seroussi H, Larour E. 2014 Deeply incised submarine glacial valleys beneath the Greenland Ice Sheet. *Nat. Geosci*. **7**, 418–422. (doi:10.1038/ngeo2167)
55. Goelzer H *et al*. 2018 Design and results of the ice sheet model initialisation experiments initMIP-Greenland: an ISMIP6 intercomparison. *The Cryosphere* **12**, 1433–1460. (doi:10.5194/tc-12-1433-2018)
56. Goelzer H *et al*. 2020 The future sea-level contribution of the Greenland ice sheet: a multi-model ensemble study of ISMIP6. *The Cryosphere* **14**, 3071–3096. (doi:10.5194/tc-14-3071-2020)
57. Seroussi H *et al*. 2020 ISMIP6 Antarctica: a multi-model ensemble of the Antarctic ice sheet evolution over the 21st century. *The Cryosphere* **14**, 3033–3070. (doi:10.5194/tc-14-3033-2020)
58. Seroussi H *et al*. 2023 Insights into the vulnerability of Antarctic glaciers from the ISMIP6 ice sheet model ensemble and associated uncertainty. *The Cryosphere* **17**, 5197–5217. (doi:10.5194/tc-17-5197-2023)
59. Seroussi H *et al*. 2024 Evolution of the Antarctic ice sheet over the next three centuries from an ISMIP6 model ensemble. *Earths. Future* **12**, e2024EF004561. (doi:10.1029/2024EF004561)
60. Morlighem M, Rignot E, Seroussi H, Larour E, Ben Dhia H, Aubry D. 2011 A mass conservation approach for mapping glacier ice thickness. *Geophys. Res. Lett* **38**, 75–83. (doi:10.1029/2011GL048659)
61. Morlighem M. 2022 MEaSUREs BedMachine Antarctica, Version 3. Boulder, CO. NASA National Snow and Ice Data Center Distributed Active Archive Center [16 January 2023]. (doi:10.5067/FPSU0V1MWUB6)
62. Roberts JL *et al*. 2011 Refined broad-scale sub-glacial morphology of Aurora Subglacial Basin, East Antarctica derived by an ice-dynamics-based interpolation scheme. *The Cryosphere* **5**, 551–560. (doi:10.5194/tc-5-551-2011)
63. MacKie EJ, Schroeder DM, Zuo C, Yin Z, Caers J. 2021 Stochastic modeling of subglacial topography exposes uncertainty in water routing at Jakobshavn Glacier. *J. Glaciol*. **67**, 75–83. (doi:10.1017/jog.2020.84)
64. Matheron G. 1963 Principles of geostatistics. *Economic Geology* **58**, 1246–1266. (doi:10.2113/gsecongeo.58.8.1246)
65. Deutsch CV, Journel AG. 1992 *GSLIB geostatistical software library and user's guide*, 2nd edn. New York, NY: Oxford University Press.
66. Mariethoz PG, Caers J. 2014 *Multiple-point geostatistics: stochastic modeling with training images*. Chichester, UK: John Wiley & Sons.
67. Yin Z, Zuo C, MacKie EJ, Caers J. 2022 Mapping high-resolution basal topography of West Antarctica from radar data using non-stationary multiple-point geostatistics (MPS-BedMappingV1). *Geosci. Model Dev*. **15**, 1477–1497. (doi:10.5194/gmd-15-1477-2022)

68. Zuo C, Yin Z, Pan Z, MacKie EJ, Caers J. 2020 A tree-based direct sampling method for stochastic surface and subsurface hydrological modeling. *Water Resour. Res.* **56**, e2019WR026130. (doi:10.1029/2019WR026130)
69. Nunes R, Soares A, Schwedersky G, Dillon L, Caetano H, Maciel C, Leon F. 2012 Geostatistical inversion of Prestack Seismic Data. In *Ninth International Geostatistics Congress*, pp. 1–8. Springer Science+Business Media Dordrecht.
70. Reuschen S, Xu T, Nowak W. 2020 Bayesian inversion of hierarchical geostatistical models using a parallel-tempering sequential Gibbs MCMC. *Adv. Water Resour*. **141**, 103614. (doi:10.1016/j.advwatres.2020.103614)
71. Shamsipour P, Marcotte D, Chouteau M, Rivest M, Bouchedda A. 2013 3D stochastic gravity inversion using nonstationary covariances. *Geophysics* **78**, G15–G24. (doi:10.1190/geo2012-0122.1)
72. Volkova A, Merkulov V. 2019 Iterative approach of gravity and magnetic inversion through geostatistics. In *Petroleum Geostatistics 2019*, Florence, Italy, vol. 2019, pp. 1–5, Florence, Italy: European Association of Geoscientists & Engineers. (doi:10.3997/2214-4609.201902257)
73. Shao N, MacKie EJ, Field MJ, McCormack FS. 2025 A Markov chain Monte Carlo approach for geostatistically simulating mass-conserving subglacial topography. *Glaciology*. (doi:10.31223/X5SB2R)
74. Cai Y, He Y, Lang S, Cui X, Zhang X, Yao Z. 2025 Siamese topographic generation model: A deep learning model for generating Antarctic subglacial topography with fine details. *Comput. Geosci*. **196**, 105857. (doi:10.1016/j.cageo.2025.105857)
75. Leong WJ, Horgan HJ. 2020 DeepBedMap: a deep neural network for resolving the bed topography of Antarctica. *The Cryosphere* **14**, 3687–3705. (doi:10.5194/tc-14-3687-2020)
76. Ramraj S, Uzir N, Sunil R, Banerjee S. 2016 Experimenting XGBoost algorithm for prediction and classification of different datasets. *Int. J. Control Theory Appl* **9**, 651–662.
77. Yi K *et al*. Evaluating machine learning and statistical models for Greenland subglacial bed topography. In *2023 International Conference on Machine Learning and Applications (ICMLA)*, Jacksonville, FL, pp. 659–666. IEEE. (doi:10.1109/ICMLA58977.2023.00097)
78. Liu Z, Rahnemoonfar M. 2025 Accurate 3D reconstruction of ice-bed topography via graph transformer. In *Algorithms for Synthetic Aperture Radar Imagery XXXII*, Orlando, FL, vol. 13456, pp. 19–26. Orlando, FL: SPIE. (doi:10.1117/12.3053945)
79. Tapoglou E, Karatzas GP, Trichakis IC, Varouchakis EA. 2014 A spatio-temporal hybrid neural network-Kriging model for groundwater level simulation. *J. Hydrol.* **519**, 3193–3203. (doi:10.1016/j.jhydrol.2014.10.040)
80. Tyralis H, Papacharalampous G. 2024 A review of predictive uncertainty estimation with machine learning. *Artif. Intell. Rev.* **57**, 94. (doi:10.1007/s10462-023-10698-8)
81. Bingham RG *et al*. 2017 Diverse landscapes beneath Pine Island Glacier influence ice flow. *Nat. Commun*. **8**, 1618. (doi:10.1038/s41467-017-01597-y)
82. Rathmann NM, Lilien DA. 2022 Inferred basal friction and mass flux affected by crystal-orientation fabrics. *J. Glaciol*. **68**, 236–252. (doi:10.1017/jog.2021.88)
83. Brinkerhoff DJ, Aschwanden A, Truffer M. 2016 Bayesian inference of subglacial topography using mass conservation. *Front. Earth Sci* **4**, 1–15. (doi:10.3389/feart.2016.00008)
84. Choi Y, Petty A, Felikson D, Poterjoy J. 2025 Estimation of the state and parameters in ice sheet model using an ensemble Kalman filter and observing system simulation experiments. *The Cryosphere* **19**, 5423–5444. (doi:10.5194/tc-19-5423-2025)
85. Gillet-Chaulet F. 2020 Assimilation of surface observations in a transient marine ice sheet model using an ensemble Kalman filter. *The Cryosphere* **14**, 811–832. (doi:10.5194/tc-14-811-2020)
86. Gudmundsson GH, Raymond M. 2008 On the limit to resolution and information on basal properties obtainable from surface data on ice streams. *The Cryosphere* **2**, 167–178. (doi:10.5194/tc-2-167-2008)
87. Morlighem M, Goldberg D. 2023 Data assimilation in glaciology. In *Applications of data assimilation and inverse problems in the earth sciences* (eds A Ismail-Zadeh, F Castelli, D Jones, S Sanchez), pp. 93–111, 1st edn. Cambridge, UK: Cambridge University Press. (doi:10.1017/9781009180412.007)

88. Thorsteinsson T, Raymond CF, Hilmar Gudmundsson G, Bindschadler RA, Vornberger P, Joughin I. 2003 Bed topography and lubrication inferred from surface measurements on fast-flowing ice streams. *J. Glaciol*. **49**, 481–490. (doi:10.3189/172756503781830502)
89. McArthur K, McCormack FS, Dow CF. 2023 Basal conditions of Denman Glacier from glacier hydrology and ice dynamics modeling. *The Cryosphere* **17**, 4705–4727. (doi:10.5194/tc-17-4705-2023)
90. Wernecke A, Edwards TL, Holden PB, Edwards NR, Cornford SL. 2022 Quantifying the impact of bedrock topography uncertainty in Pine Island Glacier projections for this century. *Geophys. Res. Lett*. **49**, e2021GL096589. (doi:10.1029/2021GL096589)
91. Gasson E, DeConto R, Pollard D. 2015 Antarctic bedrock topography uncertainty and ice sheet stability. *Geophys. Res. Lett*. **42**, 5372–5377. (doi:10.1002/2015GL064322)
92. Sun S, Cornford SL, Liu Y, Moore JC. 2014 Dynamic response of Antarctic ice shelves to bedrock uncertainty. *The Cryosphere* **8**, 1561–1576. (doi:10.5194/tc-8-1561-2014)
93. Morlighem M, Goldberg D, Dias dos Santos T, Lee J, Sagebaum M. 2021 Mapping the sensitivity of the amundsen sea embayment to changes in external forcings using automatic differentiation. *Geophys. Res. Lett*. **48**, e2021GL095440. (doi:10.1029/2021GL095440)
94. Utke J, Naumann U, Fagan M, Tallent N, Strout M, Heimbach P, Hill C, Wunsch C2008OpenAD/F: a modular open-source tool for automatic differentiation of fortran codes. *ACM Trans. Math. Softw*. **34**, 1–18. (doi:10.1145/1377596.1377598)
95. Larour E, Seroussi H, Morlighem M, Rignot E. 2012 Continental scale, high order, high spatial resolution, ice sheet modeling using the Ice Sheet System Model (ISSM). *J. Geophys. Res* **117**, F01022. (doi:10.1029/2011JF002140)
96. Smith B *et al*. 2020 Pervasive ice sheet mass loss reflects competing ocean and atmosphere processes. *Science* **368**, 1239–1242. (doi:10.1126/science.aaz5845)
97. Rignot E, Mouginot J, Scheuchl B, van den Broeke M, van Wessem MJ, Morlighem M. 2019 Four decades of Antarctic Ice Sheet mass balance from 1979–2017. *Proc. Natl Acad. Sci. USA* **116**, 1095–1103. (doi:10.1073/pnas.1812883116)
98. Bird LA, McCormack FS, Beckmann J, Jones RS, Mackintosh AN. 2025 Assessing the sensitivity of the Vanderford Glacier, East Antarctica, to basal melt and calving. *The Cryosphere* **19**, 955–973. (doi:10.5194/tc-19-955-2025)
99. Shepherd A. 2018 Mass balance of the Antarctic Ice Sheet from 1992 to 2017. *Nature* **558**, 219–222. (doi:10.1038/s41586-018-0179-y)
100. McCormack FS *et al*. 2023 Assessing the potential for ice flow piracy between the Totten and Vanderford glaciers, East Antarctica. *The Cryosphere* **17**, 4549–4569. (doi:10.5194/tc-17-4549-2023)
101. Rignot E, Mouginot J, Scheuchl B. 2011 Ice flow of the Antarctic Ice Sheet. *Science* **333**, 1427–1430. (doi:10.1126/science.1208336)
102. Rignot E, Mouginot J, Scheuchl B. 2017 MEaSUREs InSAR-based Antarctica Ice VelocityMap, Version 2. Boulder, CO. NASA National Snow and Ice Data Center Distributed Active Archive Center. See https://doi.org/10.5067/D7GK8F5J8M8R [23 November 2018]
103. Morlighem M, Seroussi H, Larour E, Rignot E. 2013 Inversion of basal friction in Antarctica using exact and incomplete adjoints of a higher-order model. *J. Geophys. Res*. **118**, 1746–1753. (doi:10.1002/jgrf.20125)
104. Glen JW. 1953 Rate of flow of polycrystalline ice. *Nature* **172**, 721–722. (doi:10.1038/172721a0)
105. Glen JW. 1955 The creep of polycrystalline ice. *Proc. R. Soc. Lond. A Math. Phys. Sci.* **228**, 519–538. (doi:10.1098/rspa.1955.0066)
106. Schoof C. 2005 The effect of cavitation on glacier sliding. *Proc. R. Soc. A*. **461**, 609–627. (doi:10.1098/rspa.2004.1350)
107. Schoof C. 2010 Coulomb friction and other sliding laws in a higher-order glacier flow model.. *Math. Models Methods Appl. Sci*. **20**, 157–189. (doi:10.1142/S0218202510004180)
108. Ehrenfeucht S, Morlighem M, Rignot E, Dow CF, Mouginot J. 2023 Seasonal acceleration of petermann glacier, Greenland, from changes in subglacial hydrology. *Geophys. Res. Lett*. **50**, e2022GL098009. (doi:10.1029/2022GL098009)
109. Rignot E, Jacobs S, Mouginot J, Scheuchl B. 2013 Ice-shelf melting around Antarctica. *Science* **341**, 266–270. (doi:10.1126/science.1235798)
110. Nowicki S *et al*. 2020 Experimental protocol for sea level projections from ISMIP6 stand-alone ice sheet models. *The Cryosphere* **14**, 2331–2368. (doi:10.5194/tc-14-2331-2020)

111. Jourdain NC, Asay-Davis X, Hattermann T, Straneo F, Seroussi H, Little CM, Nowicki S. 2020 A protocol for calculating basal melt rates in the ISMIP6 Antarctic ice sheet projections. *The Cryosphere* **14**, 3111–3134. (doi:10.5194/tc-14-3111-2020)
112. Vaňková I, Rintoul SR, Herraiz-Borreguero L, Silvano A, Greenbaum JS, van Ommen T, Jansen D, Blankenship DD. 2023 High spatial melt rate variability near the Totten Glacier grounding line in East Antarctica. *Geophys. Res. Lett.* **50**, e2023GL102960. (doi:10.1029/2023GL102960)
113. Aitken ARA, Roberts JL, van Ommen TD, Young DA, Golledge NR, Greenbaum JS, Blankenship DD, Siegert MJ. 2016 Repeated large-scale retreat and advance of Totten Glacier indicated by inland bed erosion. *Nature New Biol*. **533**, 385–389. (doi:10.1038/nature17447)
114. Pelle T, Morlighem M, McCormack FS. 2020 Aurora Basin, the Weak Underbelly of East Antarctica. *Geophys. Res. Lett* **47**, e2019GL086821. (doi:10.1029/2019GL086821)
115. Sun S, Cornford SL, Gwyther DE, Gladstone RM, Galton-Fenzi BK, Zhao L, Moore JC. 2016 Impact of ocean forcing on the Aurora Basin in the 21st and 22nd centuries. *Ann. Glaciol*. **57**, 79–86. (doi:10.1017/aog.2016.27)
116. Ehrenfeucht S, Dow C. 2025 Impacts of bed topography resolution on sea-level rise projections from coupled subglacial hydrology and ice dynamics for Thwaites Glacier, West Antarctica. *Phil. Trans. R. Soc. A* **384**, 20240545. (doi:10.1098/rsta.2024.054)
117. Badgeley JA, Morlighem M, Seroussi H. 2025 Increased sea-level contribution from northwestern Greenland for models that reproduce observations. *Proc. Natl. Acad. Sci. USA* **122**, e2411904122. (doi:10.1073/pnas.2411904122)
118. Glen JW. 1952 Experiments on the Deformation of Ice. *J. Glaciol*. **2**, 111–114. (doi:10.3189/S0022143000034067)
119. Höyns LS, Kleiner T, Rademacher A, Rückamp M, Wolovick M, Humbert A. 2025 Improved basal drag of the West Antarctic Ice Sheet from L-curve analysis of inverse models utilizing subglacial hydrology simulations. *The Cryosphere* **19**, 2133–2158. (doi:10.5194/tc-19-2133-2025)
120. Wolovick M, Humbert A, Kleiner T, Rückamp M. 2023 Regularization and L-curves in ice sheet inverse models: a case study in the Filchner–Ronne catchment. *The Cryosphere* **17**, 5027–5060. (doi:10.5194/tc-17-5027-2023)
121. Weertman J. 1957 On the sliding of glaciers. *J. Glaciol*. **3**, 33–38. (doi:10.3189/S0022143000024709)
122. Kyrke-Smith TM, Gudmundsson GH, Farrell PE. 2018 Relevance of detail in basal topography for basal slipperiness inversions: a case study on Pine Island Glacier, Antarctica. *Front. Earth Sci*. **6**. (doi:10.3389/feart.2018.00033)
123. Zoet LK, Iverson NR. 2020 A slip law for glaciers on deformable beds. *Science* **368**, 76–78. (doi:10.1126/science.aaz1183)
124. McCormack FS, Roberts JL, Dow CF, Stål T, Halpin JA, Reading AM, Siegert MJ. 2022 Fine-scale geothermal heat flow in antarctica can increase simulated subglacial melt estimates. *Geophys. Res. Lett*. **49**, e2022GL098539. (doi:10.1029/2022GL098539)
125. Reading AM, Stål T, Halpin JA, Lösing M, Ebbing J, Shen W, McCormack FS, Siddoway CS, Hasterok D. 2022 Antarctic geothermal heat flow and its implications for tectonics and ice sheets. *Nat. Rev. Earth Environ*. **3**, 814–831. (doi:10.1038/s43017-022-00348-y)
126. Smith-Johnsen S, Schlegel NJ, de Fleurian B, Nisancioglu KH. 2020 Sensitivity of the Northeast Greenland Ice Stream to Geothermal Heat. *J. Geophys. Res* **125**, e2019JF005252. (doi:10.1029/2019JF005252)
127. Thoma M, Mayer C, Grosfeld K. 2008 Sensitivity of subglacial Lake Vostok's flow regime on environmental parameters. *Earth Planet. Sci. Lett*. **269**, 242–247. (doi:10.1016/j.epsl.2008.02.023)
128. Bougamont M, Christoffersen P, Price SF, Fricker HA, Tulaczyk S, Carter SP. 2015 Reactivation of Kamb Ice Stream tributaries triggers century-scale reorganization of Siple Coast ice flow in West Antarctica. *Geophys. Res. Lett.* **42**, 8471–8480. (doi:10.1002/2015GL065782)
129. McCormack FS, Stål T, Shao N, MacKie E, Fabela Hinojosa A, Lösing M, Roberts J, Ehrenfeucht S, Dow C. 2026 Supplementary material from: Synthetic bed topographies for Antarctica and their utility in ice sheet modelling. Figshare. (doi:10.6084/m9.figshare.c.8426934)